

Efficient Hybrid Transformer: Learning Global-local Context for Urban Sence Segmentation

Libo Wang ¹, Shenghui Fang ^{1*}, Ce Zhang ^{2,3}, Rui Li ¹ and Chenxi Duan ⁴

- 1) School of Remote Sensing and Information Engineering, Wuhan University, 129 Luoyu Road, Wuhan, Hubei 430079, China.
- 2) Lancaster Environment Centre, Lancaster University, Lancaster LA1 4YQ, UK.
- 3) UK Centre for Ecology & Hydrology, Library Avenue, Lancaster LA1 4AP, UK.
- 4) Faculty of Geo-Information Science and Earth Observation (Lyons et al.), University of Twente, Enschede, the Netherlands

*Corresponding author.

Abstract—Semantic segmentation of fine-resolution urban scene images plays a vital role in extensive practical applications, such as land cover mapping, urban change detection, environmental protection and economic assessment. Driven by rapid developments in deep learning technologies, the convolutional neural network (CNN) has dominated the semantic segmentation task for many years. Convolutional neural networks adopt hierarchical feature representation, demonstrating strong local information extraction. However, the local property of the convolution layer limits the network from capturing global context that is crucial for precise segmentation. Recently, Transformer comprise a hot topic in the computer vision domain. Transformer demonstrates the great capability of global information modelling, boosting many vision tasks, such as image classification, object detection and especially semantic segmentation. In this paper, we propose an efficient hybrid Transformer (EHT) for real-time urban scene segmentation. The EHT adopts a hybrid structure with and CNN-based encoder and a transformer-based decoder, learning global-local context with lower computation. Extensive experiments demonstrate that our EHT has faster inference speed with competitive accuracy compared with state-of-the-art lightweight models. Specifically, the proposed EHT achieves a 66.9% mIoU on the UAVid test set and outperforms other benchmark networks significantly. The code will be available soon.

Index Terms—Semantic Segmentation, Transformer, Global-local Context, Hybrid Structure.

1. Introduction

Benefiting from the advance of sensor technology, more and more urban scene images are captured at fine spatial resolutions. Fine-resolution urban scene images, which contain rich semantic content and massive spatial details, play a crucial role in semantic segmentation. Semantic segmentation is a pixel-level classification task, which has extensive urban applications, including land cover mapping (Zhang et al., 2020a; Zhang et al., 2020b), change detection (Yin et al., 2018), environment protection (Samie et al., 2020), road and building extraction (Griffiths and Boehm, 2019; Shamsolmoali et al., 2020), and other practical applications (Kemker et al., 2018; Li et al., 2021a; Li et al., 2021b; Li et al., 2021c; Liu et al., 2018; Wang et al., 2021a; Wang et al., 2021b; Yang et al., 2021). Driven by deep learning technology (LeCun et al., 2015), the convolutional neural network (CNN) has dominated the semantic segmentation task for many years (Chen et al., 2014; Zhao et al., 2017; Zhu et al., 2017) (Chen et al., 2018b). In comparison with the traditional machine learning methods, such as support vector machine (SVM) (Guo et al., 2018), random forest (Pal, 2005), and conditional random field (CRF) (Krähenbühl and Koltun, 2011), CNN-based methods could capture fine-grained local context, demonstrating stronger discrimination capability.

However, CNN-based methods encounter bottlenecks when labelling fine-resolution urban scene images. Firstly, CNN-based methods lack the ability of global contextual information modelling due to the local property of convolutions. The interaction of the global and local information is critical for differentiating the complex and confusing man-made objects in the urban area, as illustrated in **Fig. 1**. Secondly, the current attention-based convolutional neural

networks cost huge computation and memory for global context capturing (Li et al., 2021d), which

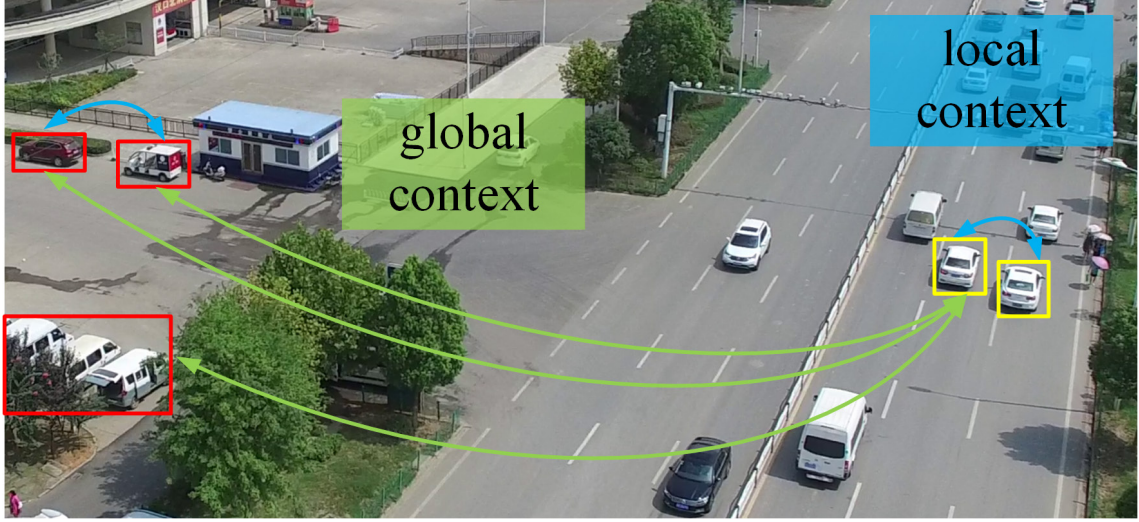


Fig. 1. Illustration of the global and local context.

reduces the efficiency and restrict its potential in urban applications.

In this paper, we aim to achieve precise urban scene segmentation while ensuring the efficiency of the network simultaneously. Inspired by the huge breakthrough obtained by the Transformer, we propose an efficient hybrid transformer (EHT) to address this challenge. Specifically, we design a global-local transformer block (GLTB). Different from the standard transformer block, the proposed GLTB constructs an attentional global branch and a convolutional local branch in the attention block to maintain the globality and locality for visual perception, as illustrated in **Fig. 2**. We introduce the window-based multi-head self-attention to realize high speed and low memory (Liu et al., 2021). To strengthen the interaction of global context and local context, we develop a cross-shaped context interaction module. In addition, we propose a feature refinement head (FRH) to further increase the segmentation accuracy. The efficiency-accuracy trade-offs and

effective feature refinement allow our method to exceed the state-of-the-art networks for efficient urban scene segmentation on three public datasets, e.g. UAVid dataset (Lyu et al., 2020), ISPRS Vaihingen dataset and Potsdam dataset.

The remainder of this paper is as follows. In Section 2, we review the related work on efficient urban scene segmentation and global contextual modelling. In Section 3, we present the structure of our EHT and introduce the proposed GLTB and FRH. In Section 4, we conduct the ablation study to demonstrate the effectiveness of GLTB and FRH and show comparison results with other state-of-the-art models on the three datasets. In Section 5, we provide a comprehensive discussion. In Section 6, we summarize the conclusions.

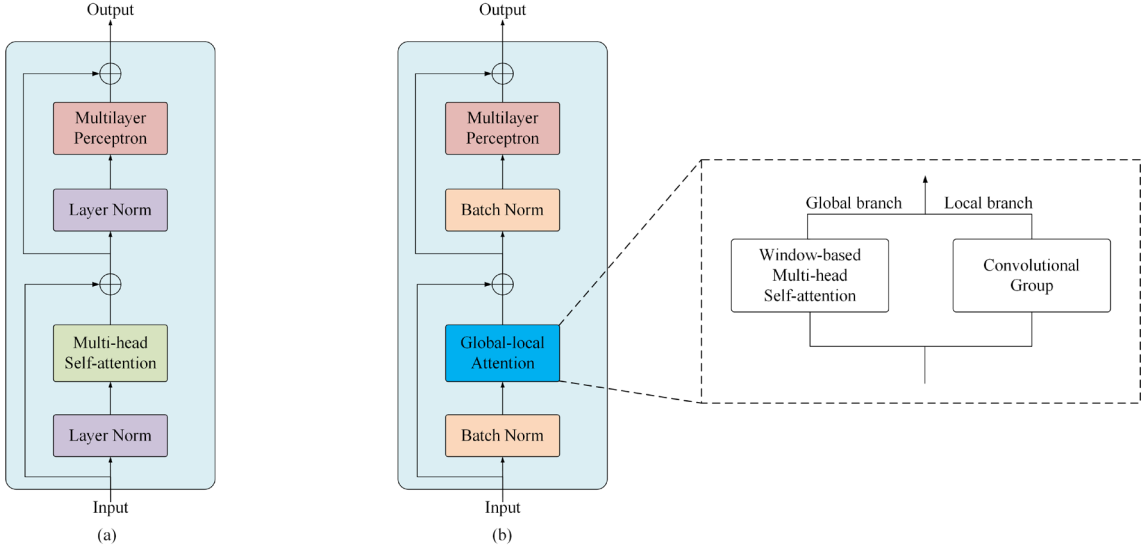


Fig. 2 Illustration of (a) the standard transformer block and (b) the global-local transformer block.

2. Related work

Semantic segmentation is one of the fundamental approaches for urban scene interpretation. Driven by advances achieved by the convolutional neural network, massive CNN-based methods are developed for boosting the accuracy of semantic segmentation (Chen et al., 2017; Maggiori

et al., 2016; Sherrah, 2016). Particularly, since the fully convolutional network (FCN) is proposed (Long et al., 2015), CNN-based methods completely dominate the semantic segmentation task (Yang et al., 2021). FCN is the first effective CNN structure to address the semantic segmentation problem in an end-to-end manner. However, the over-simplified decoder of FCN leads to a coarse-resolution segmentation, restricting the improvement of accuracy. Afterwards, many well-designed encoder-decoder networks have been presented, with two symmetric paths, namely the contracting path and the expanding path (Badrinarayanan et al., 2017; Chen et al., 2018a). The contracting extracts hierarchical features by gradually downsampling the resolution of feature maps, while the expanding path could learn more contextual information via progressively restoring the resolution (Li et al., 2021c). Representative methods like UNet perform skip pathways between the encoder and decoder for feature aggregation (Ronneberger et al., 2015), while its variant networks design elaborate skip connections to capture more abundant context (Diakogiannis et al., 2020; Li et al., 2021a; Li et al., 2021b; Zhou et al., 2018).

Complicated and confusing man-made objects frequently occurs in fine-resolution urban scene images, which seriously affects the recognition capability of CNN-based segmentation networks (Audebert et al., 2018). To address this issue, many researchers focus on modelling global contextual information to liberate the network from the local patterns of CNN. Introducing attention mechanisms into networks is the most popular way for global context capturing. Wang et al. modifies the dot-product attention and applies it to computer vision domains (Wang et al., 2018). Fu et al. append two types of attention modules on top of dilated FCN to adaptively integrate local features with their global dependencies (Fu et al., 2019). Chen et al. propose a

double attention block that adopts the gather-distribution pattern to aggregate informative global features (Chen et al., 2018c). Yuan et al. develop an object context block for exploring object-based global relations (Yuan et al., 2020). Furthermore, many attempts have been made to apply the Transformer for global information extraction (Vaswani et al., 2017). Different from the CNN structure, the Transformer translates 2D image-based tasks into 1D sequence-based tasks. Due to the powerful sequence-to-sequence modelling, the Transformer demonstrates prior in global context capturing than the above-mentioned attention-alone models and obtains state-of-the-art results on fundamental vision tasks, such as image classification (Dosovitskiy et al., 2020), objection detection (Zhu et al., 2020) and semantic segmentation (Zheng et al., 2021).

However, the huge computation complexity of the multi-head self-attention in Transformer seriously affects its potential and feasibility for urban application. To improve efficiency, several approaches abandon the pure transformer architecture and adopt the hybrid structure that combines the convolutional blocks and transformer blocks. Typical models include the bottleneck transformer (Srinivas et al., 2021), the CNNs meet transformer (CMT) (Guo et al., 2021) and the bilateral awareness network (BANet) (Wang et al., 2021b). Some research focuses on developing efficient attention mechanisms (Kitaev et al., 2020). For example, Zhang et al. reduce the resource demand by performing self-attention operations on down-sampled feature maps (Zhang and Yang, 2021). Xu et al. devise a convolution-attentional mechanism to enhance multi-scale context modelling while realizing a convolution-like efficiency (Xu et al., 2021). Recent Swin Transformer restricts self-attention within each local window and deploys a shifted operation to min the relationships between windows (Liu et al., 2021). This window-based multi-head self-

attention demonstrates linear computational complexity and superior global context modelling, surpassing previous state-of-the-art networks by a large margin.

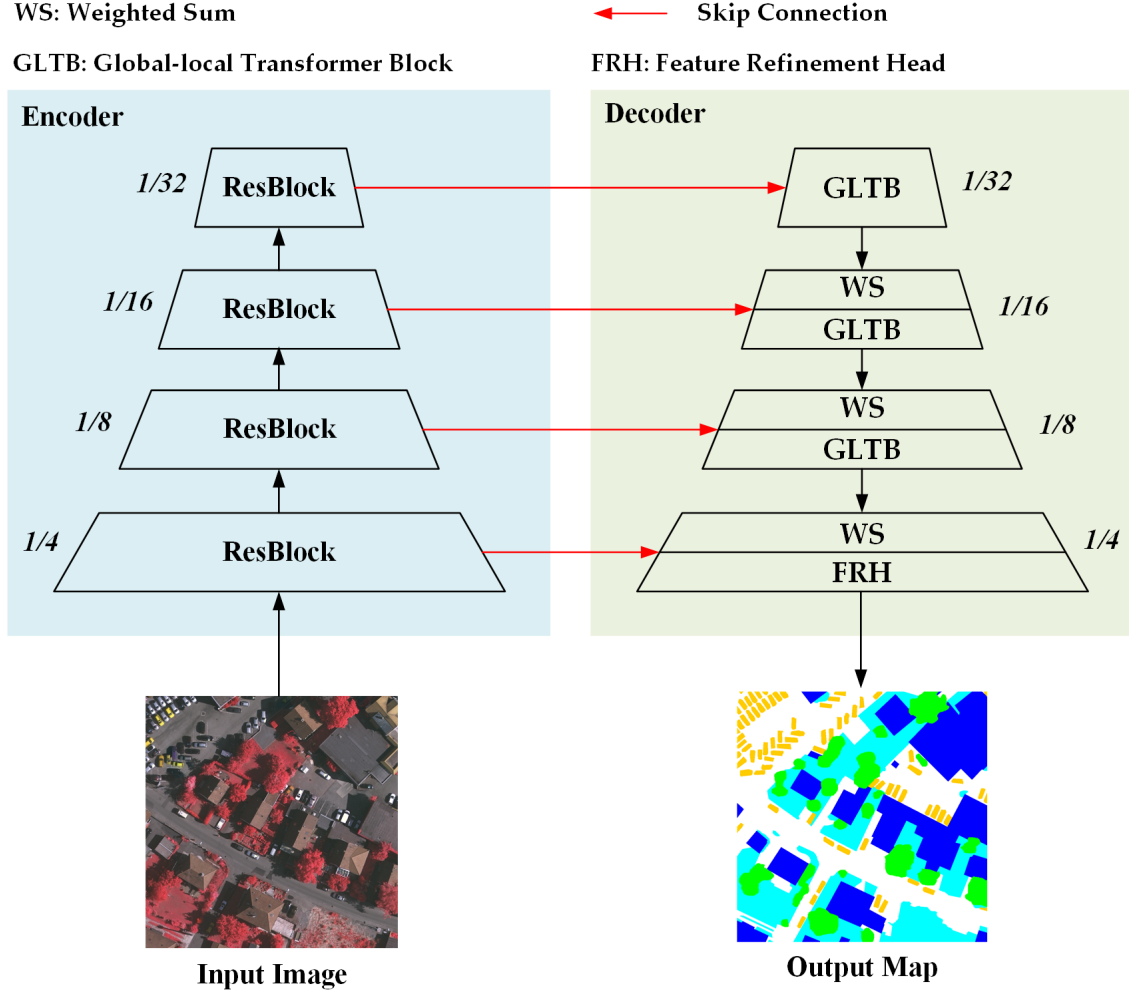


Fig. 3. An overview of the efficient hybrid transformer.

3. Efficient Hybrid Transformer

We illustrate our efficient hybrid transformer in **Fig. 3**, which is constructed by a CNN-based encoder and a transformer-based decoder. The detail of each component is illustrated in the following sections.

3.1 CNN-based encoder

The convolutional neural network ResNet18 demonstrates effectiveness and efficiency simultaneously, widely used in efficient semantic segmentation tasks. It consists of four-stage Resblocks and each stage down-samples the feature map with a scale factor of 2. We select the pre-trained ResNet18 as the encoder, which could extract multi-scale semantic features with significantly low computations. Each skip connection between the encoder and decoder is constructed by a 1×1 convolution with a channel dimension of 128. The semantic features produced by the Resblocks are further aggregated with the features generated by the GLTB using a weighted sum operation. The weighted sum operation could selectively weigh the two features in their contribution to segmentation accuracy, thereby learning a more generalized fusion feature (Tan et al., 2020).

3.2 Transformer-based decoder

Current attention modules are usually introduced into neural networks like plug-ins, extracting global scene semantics at a single scale. Differently, we utilize three global-local transformer blocks, three weighted sum operations and a feature refinement head to build a transformer-based decoder. Benefiting from this hierarchical design, the decoder could capture global context at multiple scales, demonstrating stronger feature representation.

3.1.1 Global-local transformer block (GLTB)

The Global-Local transformer block consists of the global-local attention, multilayer perceptron, two batch normalization layers and two addition operations, as shown in **Fig. 2 (b)**.

Global-local attention: The main module global-local attention constructs two branches, the local branch, while the global branch Finally, we apply a cross-shaped context interaction module to produce the global-local context. Although the global context is crucial for recognizing complex man-made objects in the urban area, the local information still needs to be preserved for describing spatial details. In this regard, the proposed global-local attention constructs two parallel branches to extract the global context and local context, respectively, as shown in **Fig. 4**.

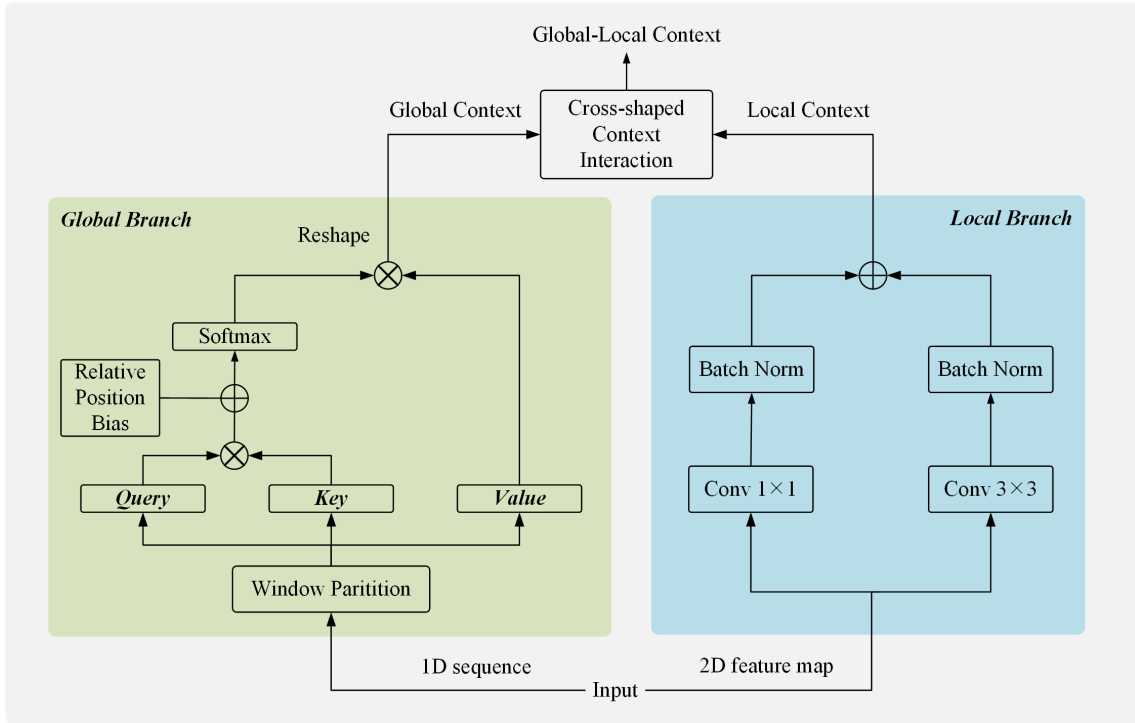


Fig. 4. The structure of the Global-local attention.

The local branch employs two parallel convolutional layers with kernel sizes of 3 and 1 to extract local context. Two batch normalization operations are attached after the convolutional layers. Finally, a sum operation is deployed to merge the extracted features.

The global branch deploys the window-based multi-head self-attention to capture global context. The input 2D feature map is first translated into a 1D sequence by a standard 1×1

convolution and a flattening operation. Then, the window partition operation split the sequence into the query (Q), key (K) and value (V) vectors. The formulation of the window-based multi-head self-attention can be denoted as:

$$\text{Attention}(\mathbf{Q}, \mathbf{K}, \mathbf{V}) = \text{SoftMax}\left(\frac{\mathbf{Q}\mathbf{K}^T}{\sqrt{d}} + B\right)\mathbf{V}, \quad (1)$$

Where $\mathbf{Q}, \mathbf{K}, \mathbf{V} \in \mathbb{R}^{W^2 \times d}$, W represents the window size and d is the channel dimension of the three vectors. W is set to 8 as default. To enhance the sequence-based modelling, we follow the previous works (Dosovitskiy et al., 2020) and introduce a relative position bias $B \in \mathbb{R}^{W^2 \times W^2}$ when computing the similarity of \mathbf{Q} and \mathbf{K} .

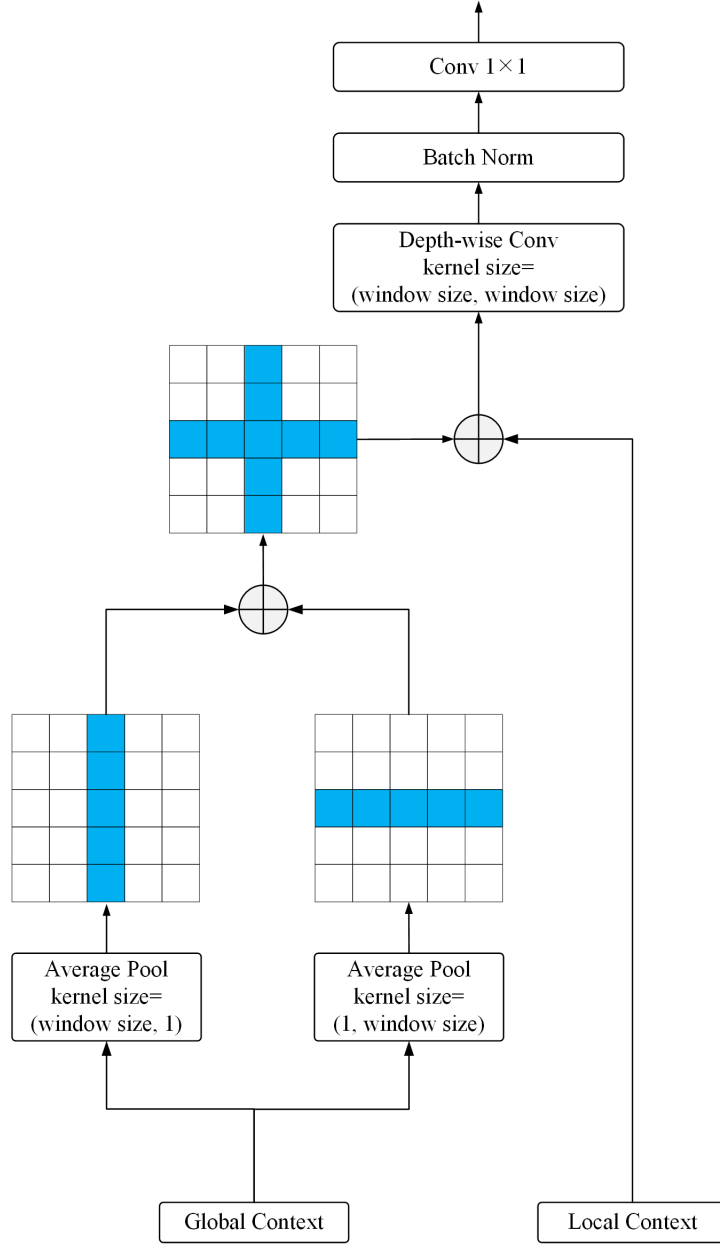


Fig. 5. The cross-shaped context interaction module.

Performing self-attention in a non-overlap local window, although efficiency, limits the modelling power due to the lack of interactions across windows. To address it, we propose a cross-shaped context interaction module, as illustrated in **Fig. 5**. The cross-shaped context interaction module fuses the two feature maps produced by a horizontal average pooling layer and a vertical average pooling layer to improve the cross-window relations. Besides, to leverage the advantages

of local semantic information, the fused cross-shaped context is further aggregated with the local context. Finally, we employ a $W \times W$ depth-wise convolution, a batch normalization operation and a standard 1×1 convolution to generate a fine-grained global-local context.

3.1.2 Feature refinement head (FRH)

The shallow feature produced by the first Resblock preserves rich segmentation details but lacks semantic content, while the deep global-local feature provides precise semantic information but presents a coarse resolution. Hence, a direct sum operation of these two features, although boosts the speed, causes damage to the segmentation accuracy (Poudel et al., 2018; Poudel et al., 2019; Yu et al., 2018). In this paper, we develop a feature refinement head to shrink the semantic gap within the two features for accurate segmentation, as illustrated in **Fig. 6**.

Firstly, we perform a weighted sum operation on the two features to take full advantage of precise semantic information and spatial details.

Secondly, we construct two paths to strengthen the channel-wise and spatial-wise feature representation. Specifically, the channel path employs a global average pooling layer to generate a channel-wise attentional map $C \in \mathbb{R}^{1 \times 1 \times c}$, where c denotes the channel dimension. The reduce&expand operation contains two 1×1 convolutional layer, which first reduces the channel dimension c with a factor of 4, then expands it to the original. The spatial path utilizes a depth-wise convolution to produce a spatial-wise attentional map $S \in \mathbb{R}^{h \times w \times 1}$, where h and w represent the resolution of the feature map. The attentional features generated by the two paths are further fused using a simple sum operation.

Finally, several post-processing convolutional layers and an upsampling operation are applied

to produce the final segmentation map. Notably, a residual connection is introduced to prevent network degradation.

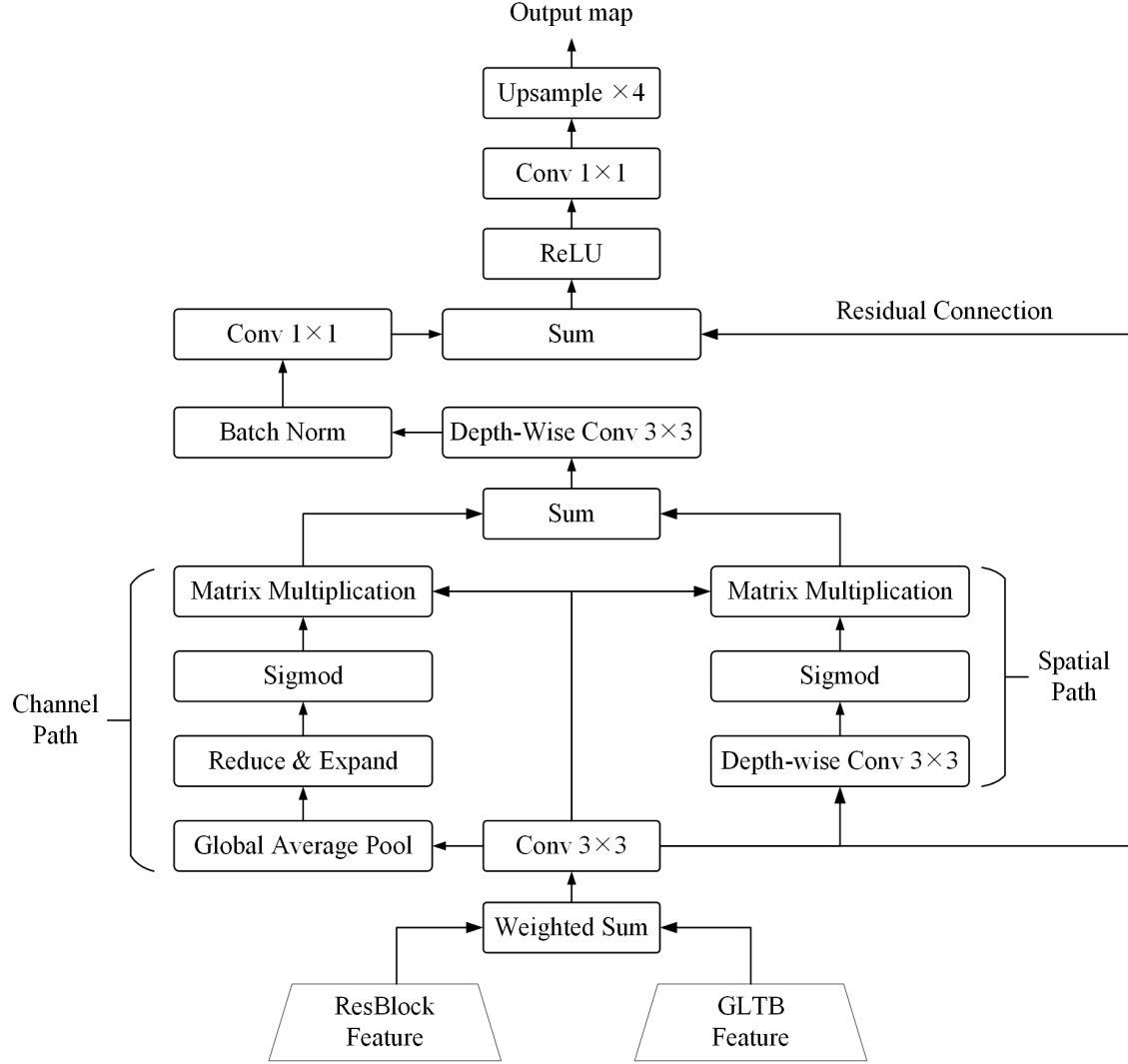


Fig. 6. The feature refinement head.

4. EXPERIMENTS

4.1 Experimental settings

4.1.1 Dataset

UAVid: As a fine-resolution Unmanned Aerial Vehicle (UAV) semantic segmentation dataset, the UAVid dataset is focusing on urban street scenes with two resolutions (3840×2160 and 4096×2160) and 8 classes. UAVid is challenging due to the large resolution of images, large-scale variation, confusing categories and complex scenes. To be specific, there are 42 sequences with a total of 420 images in the dataset, where 200 images are used for training, 70 images are used for validation and the officially provided 150 images are used for testing. In our experiments, each image is padded and cropped into four 1152×2048 px patches. The batch size is 2 and the training epoch is 40.

Vaihingen: The Vaihingen dataset consists of 33 very fine spatial resolution TOP image tiles at an average size of 2494×2064 pixels. Each TOP image tile has three multispectral bands (Near Infrared, Red, Green) as well as the digital surface model (DSM) and the normalized digital surface model (NDSM) with a 9 cm ground sampling distance (GSD). Only TOP image tiles were used in our experiments without DSM. The dataset involves five foreground classes (impervious surface, building, low vegetation, tree, car) and one background class (clutter). In our experiments, we utilized ID: 2, 4, 6, 8, 10, 12, 14, 16, 20, 22, 24, 27, 29, 31, 33, 35, 38 for testing, ID: 30 for validation, and the remaining 15 images for training. The image tiles are cropped into 1024×1024 px patches. The batch size is set to 4 and the training epoch is 30.

Potsdam: The Potsdam dataset contains 38 very fine resolution TOP image tiles (GSD 5cm) at

a size of 6000×6000 pixels and involves the same category information as the Vaihingen dataset. Four multispectral bands (Red, Green, Blue, and Near Infrared), as well as a DSM and NDSM, are provided in the dataset. We utilized ID: 2_13, 2_14, 3_13, 3_14, 4_13, 4_14, 4_15, 5_13, 5_14, 5_15, 6_13, 6_14, 6_15, 7_13 for testing, ID: 2_10 for validation, and the remaining 22 images, except for image named 7_10 with error annotations, for training.. We utilized only TOP image tiles with three bands (Red, Green, Blue) in the experiments. The cropped patches are 1024×1024 px and the batch size is 4. The training epoch is 30.

4.1.2 Implementation Details

All models in the experiments are implemented with PyTorch framework on a single NVIDIA GTX 2080ti GPU. For fast convergence, we deploy the AdamW optimizer to train all models in the experiments. The base learning rate is set to $1e-4$ and the weight decay value is 0.05. The cosine strategy is employed to adjust the learning rate and the cross-entropy loss with online hard example mining is chosen as the loss function. Random horizontal flip, random Brightness and random scale with a range of $[0.5, 2.0]$ are used for data augmentation in the training period. The test-time augmentation (TTA) strategies like horizontal flip and multiple scales $[0.75, 1.0, 1.25, 1.5, 1.75]$ are used in the test procedure.

4.1.3 Models for comparison

We select massive benchmark methods for quantitative comparison including the lightweight networks developed for efficient semantic segmentation, such as context aggregation network (CANet) (Yang et al., 2021), bilateral segmentation network (BiSeNet) (Yu et al., 2018), ,

ShelfNet (Zhuang et al., 2019) and SwiftNet (Oršić and Šegvić, 2021), Fast-SCNN (Poudel et al., 2019), DABNet (Li et al., 2019), ERFNet (Romera et al., 2017), ABCNet (Li et al., 2021d), and the attentional networks like dual attention network (DANet) (Fu et al., 2019), fast attention network (FANet) (Hu et al., 2020), multi-stage attention residual UNet (MAResU-Net) (Li et al., 2021b), and multi-attention network (MANet) (Li et al., 2021c), as well as the transformer-based networks, such as bottleneck transformer (BoTNet) (Srinivas et al., 2021) and bilateral awareness network (BANet) (Wang et al., 2021b).

4.1.4 Evaluation metrics

We use the overall accuracy (OA), mean F1 score (F1), mean intersection over union (mIoU) to evaluate the model accuracy. We use the memory footprint in MB, the multiply-add operation count (MAdds) in G, the floating point operation count (Flops) in G, the number of model parameters in M and the inference speed in frames per second (FPS) to evaluate the model efficiency.

TABLE 1. Ablation study of each component of EHT.

Dataset	Method	mIoU (LeCun et al.)
UAVid	Baseline	61.8
	Baseline + GLTB	65.6
	Baseline + GLTB + FRH	66.9
Vaihingen	Baseline	78.9
	Baseline + GLTB	81.0
	Baseline + GLTB + FRH	82.0
Potsdam	Baseline	83.1
	Baseline + GLTB	85.8
	Baseline + GLTB + FRH	86.6

4.2 Experiment results

4.2.1 Ablation study

To evaluate the performance of the GLTB and FRH separately, we conduct ablation experiments on the three datasets. The results are illustrated in **TABLE 1**.

Baseline: The baseline is constructed by the UNet with a ResNet18 backbone.

Ablation study for global-local transformer block: We introduce three global-local transformer blocks into the baseline to construct a simple variant (denoted as **Baseline + GLTB**). The deployment of GLTB provides a significant improvement of mIoU by 3.8% on the UAVid test set and achieves an increase of greater than 2.1% in mIoU on the Vaihingen and Potsdam test

sets, which demonstrates the effectiveness of GLTB.

TABLE 2. The complexity and speed of the proposed EHT and other lightweight methods. We choose a 1024×2048 px patch as the input image and report the inference speed measured in frames per second (FPS) on a NVIDIA GTX 2080ti GPU.

Method	Backbone	Flops(G)	Memory(MB)	MAdd(G)	Parameters(M)	FPS	mIoU
Fast-SCNN	-	6.72	1239.33	13.85	1.14	128.97	45.9
BiSeNet	ResNet18	103.72	1941.39	208.18	12.89	65.50	61.5
DANet	ResNet18	79.20	1222.36	158.22	12.67	65.54	60.6
FANet	ResNet18	173.72	1949.64	347.14	13.67	30.99	-
ShelfNet	ResNet18	93.69	1158.12	187.37	14.6	44.37	47.0
SwiftNet	ResNet18	103.37	1671.66	207.64	11.80	45.40	61.1
MANet	ResNet18	103.33	2338.33	242.94	12.0	23.27	62.6
ABCNet	ResNet18	125.95	2210.25	251.50	14.06	35.41	63.8
BoTNet	ResNet18	90.52	1352.50	180.82	17.69	54.08	63.2
EHT	ResNet18	89.00	1962.00	177.70	11.65	44.18	66.9

Ablation study for the cross-scale fusion module: We inserted the feature refinement head into **Baseline + GLTB** to generate the entire EHT (indicated as **Baseline + GLTB + FRH**). With the employment of FRH, the mIoU is boosted by 1% at least, demonstrating the validity of the proposed feature refinement module.

4.2.2 Comparison of model efficiency

The complexity and inference speed are critical for evaluating a network, especially in urban applications. We compare our EHT with efficient segmentation networks based on the mIoU, GPU memory footprint, MAdds, Flops, model parameters and inference speed on the official UAVid test set. The comparison results are listed in **Table 2**. In comparison with the fastest and most tiny model Fast-SCNN, the proposed EHT outperforms it by a large margin of 21.0% in mIoU. In comparison with the state-of-the-art models of the same volume, our EHT could achieve a competitive inference speed of 44.18 FPS, while surpassing other networks by more than 3.1% in mIoU. The outstanding trade-off between accuracy and speed demonstrates the effectiveness and efficiency of our transformer-based decoder composed of GLTB and FRH.

TABLE 3. Quantitative comparison results on the UAVid test set with lightweight models.

The best values in the column are in bold.

Method	Backbone	Clutter	Building	Road	Tree	Vegetation	Moving Car	Static Car	Human	mIoU
MSD	-	57.0	79.8	74.0	74.5	55.9	62.9	32.1	19.7	57.0
CANet	-	66.0	86.6	62.1	79.3	78.1	47.8	68.3	19.9	63.5
DANet	ResNet18	64.9	85.9	77.9	78.3	61.5	59.6	47.4	9.1	60.6
SwiftNet	ResNet18	64.1	85.3	61.5	78.3	76.4	51.1	62.1	15.7	61.1
BiSeNet	ResNet18	64.7	85.7	61.1	78.3	77.3	48.6	63.4	17.5	61.5
MANet	ResNet18	64.5	85.4	77.8	77.0	60.3	67.2	53.6	14.9	62.6
ABCNet	ResNet18	67.4	86.4	81.2	79.9	63.1	69.8	48.4	13.9	63.8
BANet	ResT-lite	66.7	85.4	80.7	78.9	62.1	69.3	52.8	21.0	64.6
BoTNet	ResNet18	64.5	84.9	78.6	77.4	60.5	65.8	51.9	22.4	63.2
EHT	ResNet18	67.8	87.5	81.2	80.2	64.2	71.9	58.9	23.6	66.9

4.2.3 Results on the UAVid dataset

UAVid is a large-scale urban scene segmentation dataset, where the images are captured by unmanned aerial vehicles in different cities and under different lighting conditions. Thus, it is not easy to obtain a high score on such a challenging dataset. We train several advanced efficient segmentation networks and report detailed comparison results on the official UAVid test set. As illustrated in **Table 3**, our method yields the best mIoU (66.9%) while maintaining advantages in the per-class IoU. Specifically, the proposed EHT not only exceeds the well-designed CNN-based

model ABCNet by 3.1% in m IoU but also outperforms the recent transformer-based network BANet and BoTNet by 2.3% and 3.7%, respectively. Particularly, the “human” class is hard to handle since it is an extremely small geo-object. Nonetheless, the IoU of this class achieved by our EHT is at least 1.2% higher than other methods. Furthermore, the segmentation results from the UAVid validation set (**Fig. 7**) and the enlarged visualization results from the the UAVid test set (**Fig. 8**) also demonstrate the effectiveness of our model.

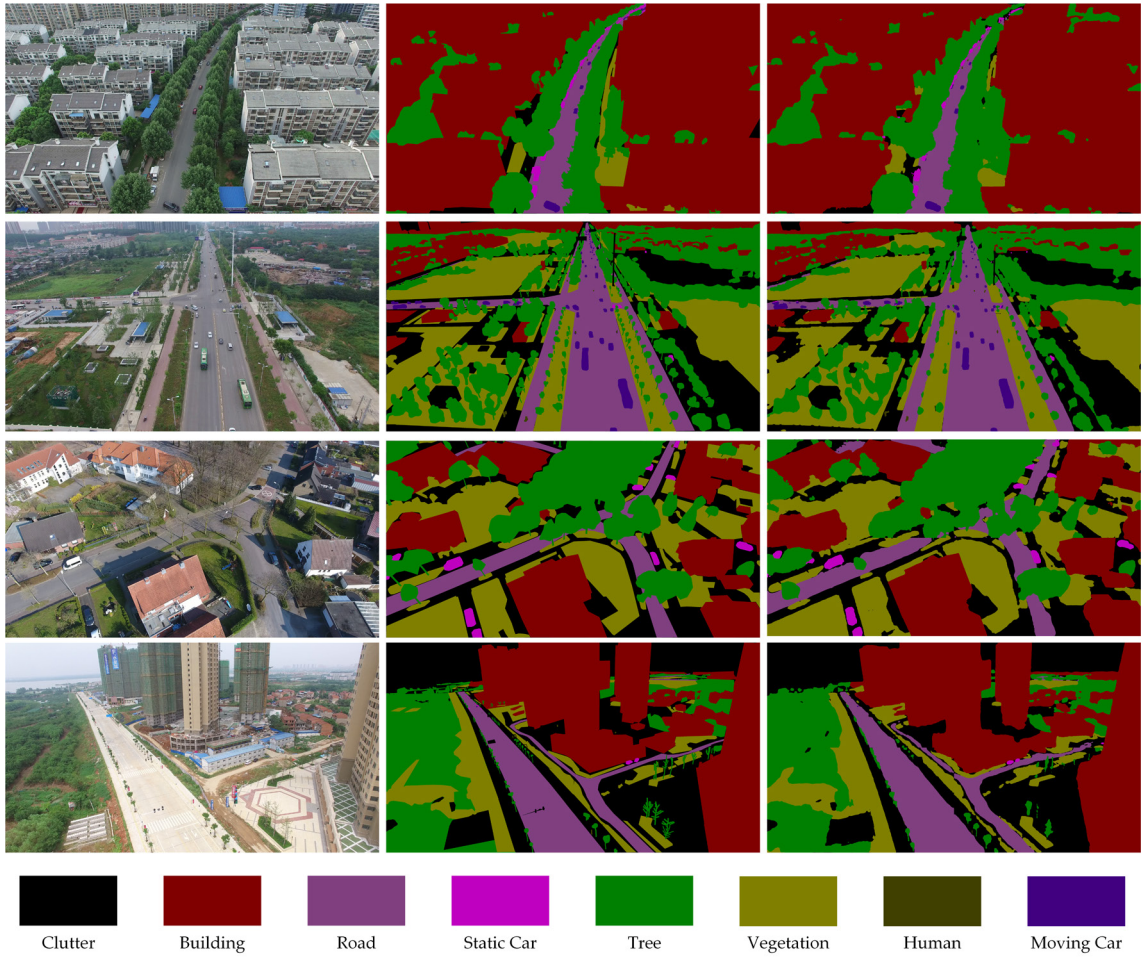


Fig. 7. Segmentation results from the UAVid validation set. The first column represents the input RGB images. The second column denotes the ground truth. The third column shows the segmentation maps of our method.

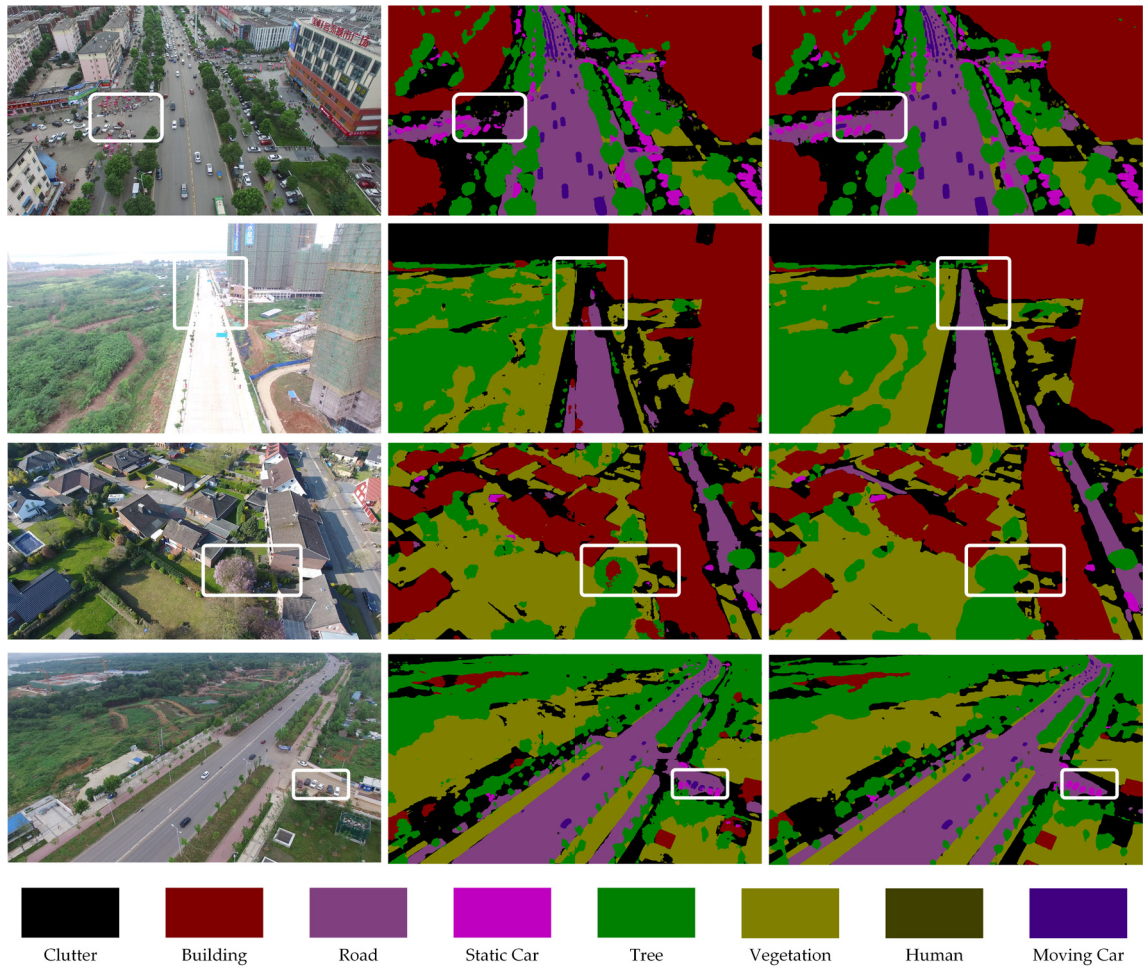


Fig. 8. Enlarged visualization of results from the UAVid test set. The first column represents the input RGB images. The second column denotes the segmentation results of the baseline. The third column shows the segmentation maps of our method.

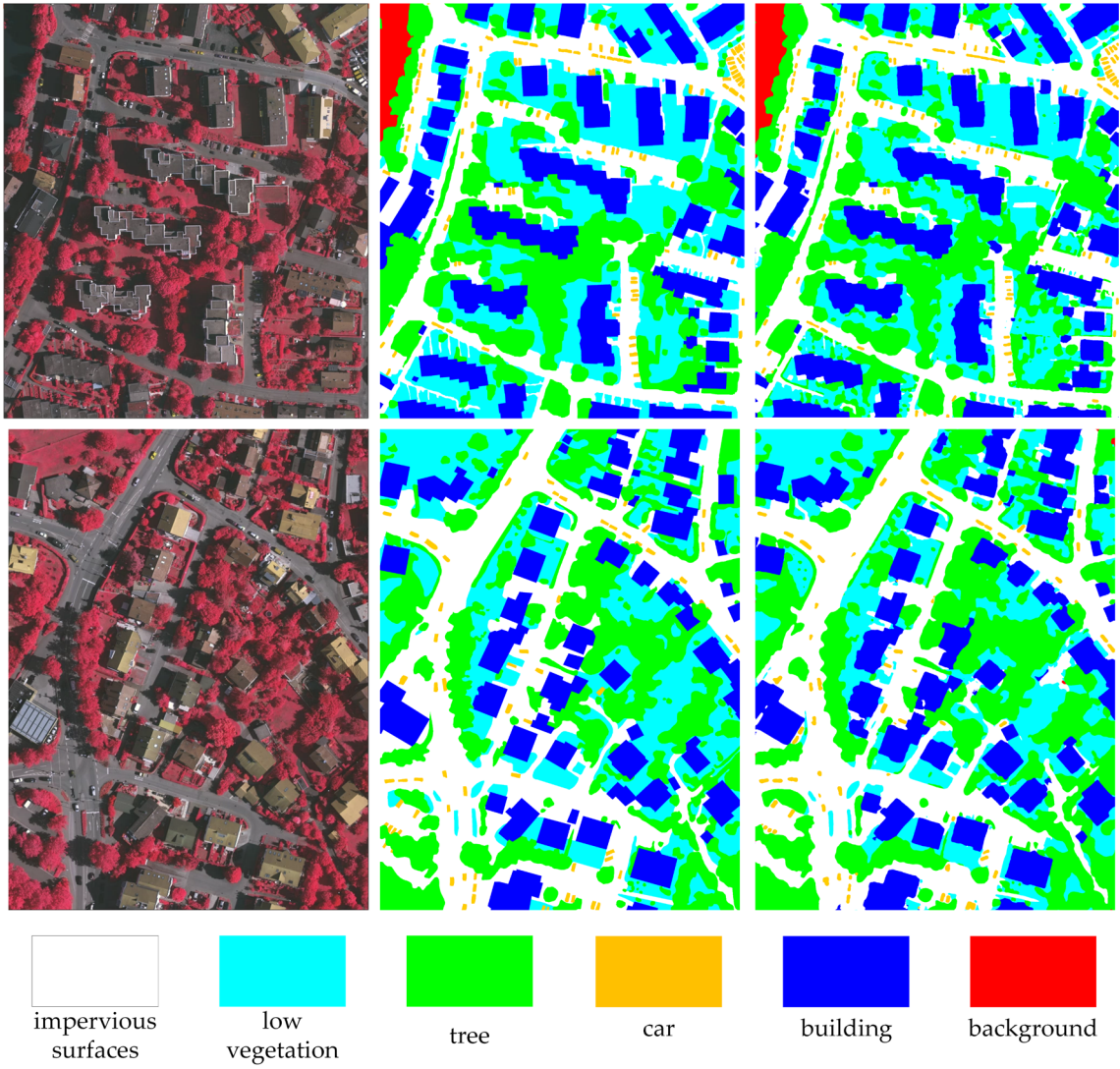


Fig. 9. Visualization results of ID 2 and 22 from the Vaihingen test set. The first column denotes the input RGB images. The second column represents the ground truth. The third column shows the segmentation results of the proposed EHT.

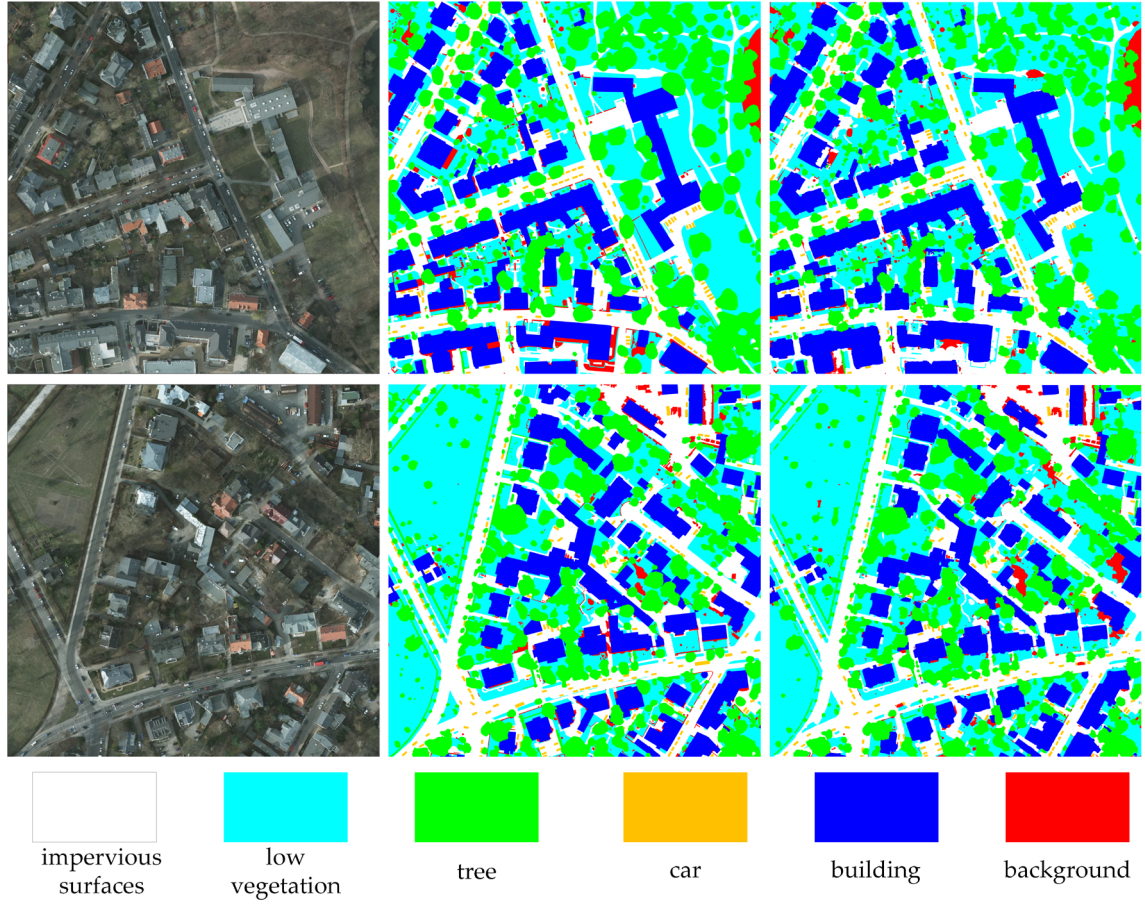


Fig. 10. Visualization results of ID 3_14 and 2_13 from the Potsdam test set. The first column denotes the input RGB images. The second column represents the ground truth. The third column shows the segmentation results of the proposed EHT.

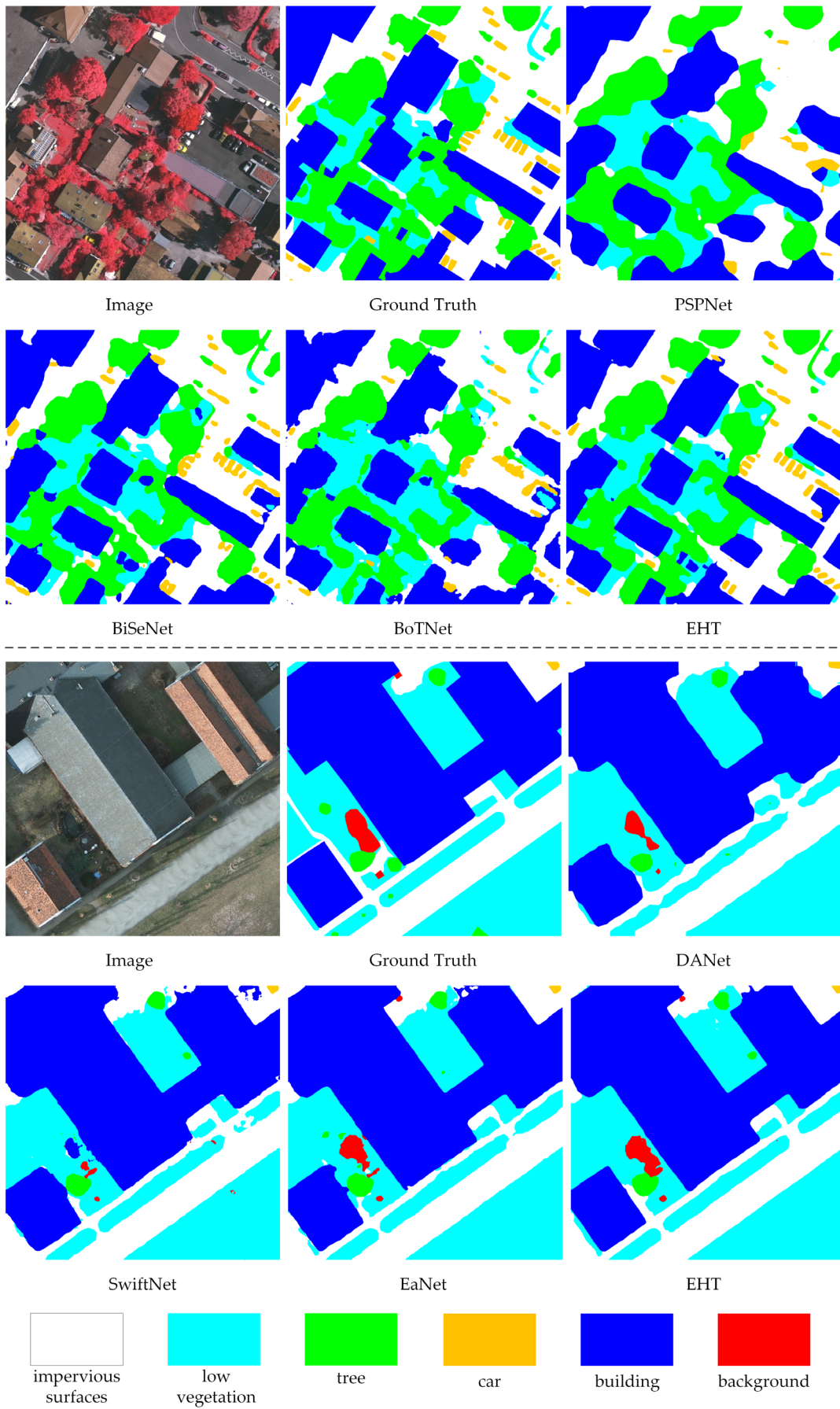


Fig. 11. Enlarged visualization of results from the Vaihingen (top) and Potsdam (bottom) test set.**TABLE 4.** Quantitative comparison results on the Vaihingen test set with the lightweight networks. The best values are in bold.

Method	Backbone	Imp. surf.	Building	Low veg.	Tree	Car	Mean F1	OA	mIoU
DABNet	-	87.8	88.8	74.3	84.9	60.2	79.2	84.3	70.2
ERFNet	-	88.5	90.2	76.4	85.8	53.6	78.9	85.8	69.1
BiSeNet	ResNet18	89.1	91.3	80.9	86.9	73.1	84.3	87.1	75.8
PSPNet	ResNet18	89.0	93.2	81.5	87.7	43.9	79.0	87.7	68.6
DANet	ResNet18	90.0	93.9	82.2	87.3	44.5	79.6	88.2	69.4
FANet	ResNet18	90.7	93.8	82.6	88.6	71.6	85.4	88.9	75.6
EaNet	ResNet18	91.7	94.5	83.1	89.2	80.0	87.7	89.7	78.7
ShelfNet	ResNet18	91.8	94.6	83.8	89.3	77.9	87.5	89.8	78.3
MAResU-Net	ResNet18	92.0	95.0	83.7	89.3	78.3	87.7	90.1	78.6
SwiftNet	ResNet18	92.2	94.8	84.1	89.3	81.2	88.3	90.2	79.6
BoTNet	ResNet18	89.9	92.1	81.8	88.7	71.3	84.8	88.0	74.3
EUT	ResNet18	92.7	95.4	84.4	90.3	87.1	90.0	90.8	82.0

4.2.4 Results on the Vaihingen and Potsdam dataset

The ISPRS Vaihingen and Potsdam are two widely used datasets. Numeric high accuracies are achieved by the specially designed models on these two datasets. In this section, we demonstrate that our EHT can not only surpass lightweight models but also obtain competitive scores in comparison with leading networks.

TABLE 5. Quantitative comparison results on the Vaihingen test set with the state-of-the-art networks. FPS is tested on a single NVIDIA GTX 2080Ti GPU with a input size of 1024×2048 . The best values are in bold.

Method	Backbone	Imp. surf.	Building	Low veg.	Tree	Car	Mean F1	OA	mIoU	FPS
DeepLabV3+	ResNet101	92.4	95.2	84.3	89.5	86.5	89.6	90.6	81.5	8.35
PSPNet	ResNet101	92.8	95.5	84.5	89.9	88.6	90.3	90.9	82.6	9.88
DANet	ResNe101	91.6	95.0	83.3	88.9	87.2	89.2	90.4	81.3	12.22
EaNet	ResNet101	93.4	96.2	85.6	90.5	88.3	90.8	91.2	-	7.44
DDCM-Net	ResNet50	92.7	95.3	83.3	89.4	88.3	89.8	90.4	-	14.03
HUSTW5	RessegNets	93.3	96.1	86.4	90.8	74.6	88.2	91.6	-	-
CASIA2	ResNet101	93.2	96.0	84.7	89.9	86.7	90.1	91.1	-	-
MANet	ResNe50	93.0	95.5	84.6	90.0	88.9	90.4	91.0	82.7	7.25
DLR_9	-	92.4	95.2	83.9	89.9	81.2	88.5	90.3	-	-
EUT	ResNet18	92.7	95.4	84.4	90.3	87.1	90.0	90.8	82.0	44.18

As illustrated in **Table 4**, the proposed EHT delivers the best F1, OA and mIoU on the Vaihingen test set, outperforming other lightweight networks by a significant margin. It is worth noting that our method yields an 87.1% F1 score on the “car” class, exceeding other benchmark networks by more than 5.9%. In **Table 5**, we compare our method with high-complexity state-of-the-art networks. The comparison results indicate that the proposed EHT yields a competitive accuracy with a significantly faster inference speed. Moreover, the prediction results of ID 2 and 22 are shown in **Fig. 9**, while the enlarged visualization of results is illustrated in **Fig. 11 (Top)**,

TABLE 6 Quantitative comparison results on the Potsdam test set with the lightweight networks.

Method	Backbone	Imp. surf.	Building	Low veg.	Tree	Car	Mean F1	OA	mIoU
ERFNet	-	88.7	93.0	81.1	75.8	90.5	85.8	84.5	76.2
DABNet	-	89.9	93.2	83.6	82.3	92.6	88.3	86.7	79.6
PSPNet	ResNet18	89.1	94.5	84.0	85.8	76.6	86.0	87.2	75.9
BiSeNetV1	ResNet18	90.2	94.6	85.5	86.2	92.7	89.8	88.2	81.7
BiSeNetV2	-	91.3	94.3	85.0	85.2	94.1	90.0	88.2	82.3
EaNet	ResNet18	92.0	95.7	84.3	85.7	95.1	90.6	88.7	83.4
MAResU-Net	ResNet18	91.4	95.6	85.8	86.6	93.3	90.5	89.0	83.9
DANet	ResNet18	91.0	95.6	86.1	87.6	84.3	88.9	89.1	80.3
SwiftNet	ResNet18	91.8	95.9	85.7	86.8	94.5	91.0	89.3	83.8
FANet	ResNet18	92.0	96.1	86.0	87.8	94.5	91.3	89.8	84.2
ShelfNet	ResNet18	92.5	95.8	86.6	87.1	94.6	91.3	89.9	84.4
EHT	ResNet18	93.7	97.0	87.6	88.8	96.4	92.7	91.3	86.6

which also demonstrates the effectiveness of our EHT.

For a comprehensive evaluation, we further conduct experiments on the Postdam dataset. As shown in **Table 6**, our EHT achieves a 92.7% mean F1 score and an 86.6% mIoU on the Potsdam test set and exceeds other lightweight models in all categories. Besides, our method can obtain an equivalent performance to the state-of-the-art models with high computation complexity while maintaining a much faster inference speed (**Table 7**). We also provide the segmentation results of ID 3_14 and 2_13 (**Fig. 10**) and the enlarged visualization of results (**Fig. 11**) to show the

preferential performance of our network.

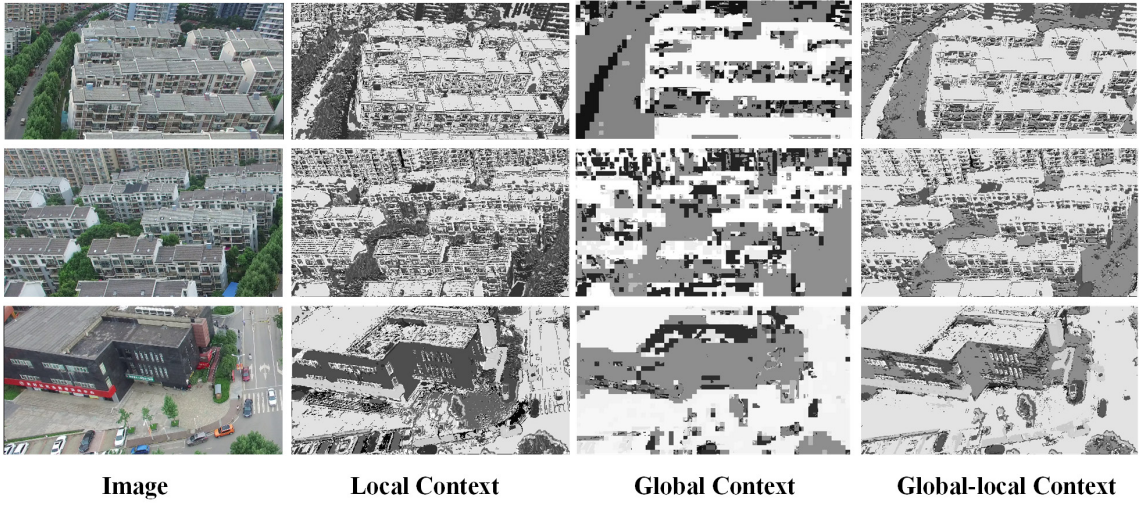


Fig. 12. Visualization results of the local context, global context and global-local context in the proposed global-local attention.

TABLE 7. Quantitative comparison results on the Potsdam test set with state-of-the-art networks. FPS is tested on a single NVIDIA GTX 2080Ti GPU with a input size of 1024×2048 . The best values are in bold.

Method	Backbone	Imp. surf.	Building	Low veg.	Tree	Car	Mean F1	OA	mIoU	FPS
DeepLabV3+	ResNet101	93.0	95.9	87.6	88.2	96.0	92.1	90.9	84.3	8.35
PSPNet	ResNet101	93.4	97.0	87.8	88.5	95.4	92.4	91.1	84.9	9.88
DDCM-Net	ResNet50	92.9	96.9	87.7	89.4	94.9	92.3	90.8	-	14.03
CCNet	ResNet101	93.6	96.8	86.9	88.6	96.2	92.4	91.5	85.7	12.19
AMA_1	-	93.4	96.8	87.7	88.8	96.0	92.5	91.2	-	-
SWJ_2	ResNet101	94.4	97.4	87.8	87.6	94.7	92.4	91.7	-	-
HUSTW4	ResegNets	93.6	97.6	88.5	88.8	94.6	92.6	91.6	-	-
V-FuseNet	FuseNet	92.7	96.3	87.3	88.5	95.4	92.0	90.6	-	-
DST_5	FCN	92.5	96.4	86.7	88.0	94.7	91.7	90.3	-	-
EHT	ResNet18	93.7	97.0	87.6	88.8	96.4	92.7	91.3	86.6	44.18

5. Discussion

The comprehensive comparison in experiments indicates the priority of our EHT in the trade-off between accuracy and efficiency. Two vital factors ensure the advanced trade-off of the EHT.

Firstly, the dual-branch structure of the proposed global-local attention could extract sufficient global context while preserving fine-grained local information. To demonstrate this, we visualize the feature maps from the two branches and the global-local context extracted by the global-local attention in **Fig. 12**. As we can see from the figure, the local context extracted by the local branch preserves the abundant local features but lacks spatial consistency. Meanwhile, the global context captured by the global branch has a more consistent character but lacks locality. Performing the self-attention operation within a local window also causes jagged edges in the global feature maps. Therefore, we employ a cross-shaped context interaction module for context aggregation. On the one hand, the cross-shaped context interaction module could fully leverage the advantages of the global context and local context, providing a global-local feature representation. On the other hand, the cross-shape context aggregation enhances the interaction between windows, resolving the jagged issue. Visibly, the extracted global-local context is superior to the global context and local context (**Fig. 12**). Furthermore, the proposed FRH narrows the semantic gap between the shallow convolutional feature and the deep global-local feature while retaining a fine-resolution representation, which further improves the segmentation accuracy.

Secondly, the proposed EHT adopts a hybrid structure with a CNN-based encoder and a transformer-based decoder. This elaborate design saves huge computation compared to pure transformer-based networks and achieves a competitive efficiency of lightweight convolutional

neural networks. Moreover, the deployment of the linear window-based multi-head self-attention further boosts the inference speed and reduces the GPU memory requirement.

6. Conclusion

In this paper, we propose a novel efficient hybrid transformer (EHT) for semantic segmentation of fine-resolution urban scene images. For accurate segmentation, we design a global-local transformer block (GLTB) to extract the global context and local context and strengthen their interaction, while develops a feature refinement head (FRH) to further improve the accuracy. For efficient segmentation, we design a hybrid architecture with a lightweight encoder and a fast transformer-based decoder. Extensive experiments on the ISPRS Vaihingen and Potsdam datasets as well as the UAVid dataset demonstrate the effectiveness and efficiency of the proposed EHT for real-time urban applications. In future work, we will continue to explore the potential and feasibility of the Transformer and develop a universal and uniform backbone for vision tasks.

Declaration of Competing Interest

The authors declare that they have no known competing financial interests or personal relationships that could have appeared to influence the work reported in this paper.

References

- Audebert, N., Le Saux, B., Lefèvre, S., 2018. Beyond RGB: Very high resolution urban remote sensing with multimodal deep networks. *ISPRS Journal of Photogrammetry and Remote Sensing* 140, 20-32.
- Badrinarayanan, V., Kendall, A., Cipolla, R., 2017. Segnet: A deep convolutional encoder-decoder architecture for image segmentation. *IEEE transactions on pattern analysis and machine intelligence* 39, 2481-2495.
- Chen, L.-C., Papandreou, G., Kokkinos, I., Murphy, K., Yuille, A.L., 2014. Semantic image segmentation with deep convolutional nets and fully connected crfs. *arXiv preprint arXiv:1412.7062*.
- Chen, L.-C., Papandreou, G., Schroff, F., Adam, H., 2017. Rethinking atrous convolution for semantic

image segmentation. arXiv preprint arXiv:1706.05587.

Chen, L.-C., Zhu, Y., Papandreou, G., Schroff, F., Adam, H., 2018a. Encoder-decoder with atrous separable convolution for semantic image segmentation, *Proceedings of the European conference on computer vision (ECCV)*, pp. 801-818.

Chen, L., Papandreou, G., Kokkinos, I., Murphy, K., Yuille, A.L., 2018b. DeepLab: Semantic Image Segmentation with Deep Convolutional Nets, Atrous Convolution, and Fully Connected CRFs. *IEEE Transactions on Pattern Analysis and Machine Intelligence* 40, 834-848.

Chen, Y., Kalantidis, Y., Li, J., Yan, S., Feng, J., 2018c. \mathcal{A}^2 -Nets: Double Attention Networks. arXiv preprint arXiv:1810.11579.

Diakogiannis, F.I., Waldner, F., Caccetta, P., Wu, C., 2020. Resunet-a: a deep learning framework for semantic segmentation of remotely sensed data. *ISPRS Journal of Photogrammetry and Remote Sensing* 162, 94-114.

Dosovitskiy, A., Beyer, L., Kolesnikov, A., Weissenborn, D., Zhai, X., Unterthiner, T., Dehghani, M., Minderer, M., Heigold, G., Gelly, S., 2020. An image is worth 16x16 words: Transformers for image recognition at scale. arXiv preprint arXiv:2010.11929.

Fu, J., Liu, J., Tian, H., Li, Y., Bao, Y., Fang, Z., Lu, H., 2019. Dual attention network for scene segmentation, *Proceedings of the IEEE Conference on Computer Vision and Pattern Recognition*, pp. 3146-3154.

Griffiths, D., Boehm, J., 2019. Improving public data for building segmentation from Convolutional Neural Networks (CNNs) for fused airborne lidar and image data using active contours. *ISPRS Journal of Photogrammetry and Remote Sensing* 154, 70-83.

Guo, J., Han, K., Wu, H., Xu, C., Tang, Y., Xu, C., Wang, Y., 2021. CMT: Convolutional Neural Networks Meet Vision Transformers. arXiv preprint arXiv:2107.06263.

Guo, Y., Jia, X., Paull, D., 2018. Effective Sequential Classifier Training for SVM-Based Multitemporal Remote Sensing Image Classification. *IEEE Transactions on Image Processing* 27, 3036-3048.

Hu, P., Perazzi, F., Heilbron, F.C., Wang, O., Lin, Z., Saenko, K., Sclaroff, S., 2020. Real-time semantic segmentation with fast attention. *IEEE Robotics and Automation Letters* 6, 263-270.

Kemker, R., Salvaggio, C., Kanan, C., 2018. Algorithms for semantic segmentation of multispectral remote sensing imagery using deep learning. *ISPRS journal of photogrammetry and remote sensing* 145, 60-77.

Kitaev, N., Kaiser, L., Levskaya, A., 2020. Reformer: The efficient transformer. arXiv preprint arXiv:2001.04451.

Krähenbühl, P., Koltun, V., 2011. Efficient inference in fully connected crfs with gaussian edge potentials. *Advances in neural information processing systems* 24, 109-117.

LeCun, Y., Bengio, Y., Hinton, G.J.n., 2015. Deep learning. *Nature* 521, 436-444.

Li, G., Yun, I., Kim, J., Kim, J., 2019. Dabnet: Depth-wise asymmetric bottleneck for real-time semantic segmentation. arXiv preprint arXiv:1907.11357.

Li, R., Duan, C., Zheng, S., Zhang, C., Atkinson, P.M., 2021a. MACU-Net for semantic segmentation of fine-resolution remotely sensed images. *IEEE Geoscience and Remote Sensing Letters*.

Li, R., Zheng, S., Duan, C., Su, J., Zhang, C., 2021b. Multistage Attention ResU-Net for Semantic Segmentation of Fine-Resolution Remote Sensing Images. *IEEE Geoscience and Remote Sensing Letters*.

Li, R., Zheng, S., Zhang, C., Duan, C., Su, J., Wang, L., Atkinson, P.M., 2021c. Multiattention network for semantic segmentation of fine-resolution remote sensing images. *IEEE Transactions on Geoscience and Remote Sensing*.

Li, R., Zheng, S., Zhang, C., Duan, C., Wang, L., Atkinson, P.M., 2021d. ABCNet: Attentive bilateral

- contextual network for efficient semantic segmentation of Fine-Resolution remotely sensed imagery. *ISPRS Journal of Photogrammetry and Remote Sensing* 181, 84-98.
- Liu, Y., Fan, B., Wang, L., Bai, J., Xiang, S., Pan, C., 2018. Semantic labeling in very high resolution images via a self-cascaded convolutional neural network. *ISPRS journal of photogrammetry and remote sensing* 145, 78-95.
- Liu, Z., Lin, Y., Cao, Y., Hu, H., Wei, Y., Zhang, Z., Lin, S., Guo, B., 2021. Swin transformer: Hierarchical vision transformer using shifted windows. *arXiv preprint arXiv:2103.14030*.
- Long, J., Shelhamer, E., Darrell, T., 2015. Fully convolutional networks for semantic segmentation, *Proceedings of the IEEE conference on computer vision and pattern recognition*, pp. 3431-3440.
- Lyons, M.B., Keith, D.A., Phinn, S.R., Mason, T.J., Elith, J., 2018. A comparison of resampling methods for remote sensing classification and accuracy assessment. *Remote Sensing of Environment* 208, 145-153.
- Lyu, Y., Vosselman, G., Xia, G.-S., Yilmaz, A., Yang, M.Y., 2020. UAVid: A semantic segmentation dataset for UAV imagery. *ISPRS Journal of Photogrammetry and Remote Sensing* 165, 108-119.
- Maggiori, E., Tarabalka, Y., Charpiat, G., Alliez, P., 2016. Convolutional neural networks for large-scale remote-sensing image classification. *IEEE Transactions on Geoscience and Remote Sensing* 55, 645-657.
- Oršić, M., Šegvić, S., 2021. Efficient semantic segmentation with pyramidal fusion. *Pattern Recognition* 110, 107611.
- Pal, M., 2005. Random forest classifier for remote sensing classification. *International Journal of Remote Sensing* 26, 217-222.
- Poudel, R.P., Bonde, U., Liwicki, S., Zach, C., 2018. Contextnet: Exploring context and detail for semantic segmentation in real-time. *arXiv preprint arXiv:1805.04554*.
- Poudel, R.P., Liwicki, S., Cipolla, R., 2019. Fast-scnn: Fast semantic segmentation network. *arXiv preprint arXiv:1902.04502*.
- Romera, E., Alvarez, J.M., Bergasa, L.M., Arroyo, R., 2017. Erfnet: Efficient residual factorized convnet for real-time semantic segmentation. *IEEE Transactions on Intelligent Transportation Systems* 19, 263-272.
- Ronneberger, O., Fischer, P., Brox, T., 2015. U-net: Convolutional networks for biomedical image segmentation, *International Conference on Medical image computing and computer-assisted intervention*. Springer, pp. 234-241.
- Samie, A., Abbas, A., Azeem, M.M., Hamid, S., Iqbal, M.A., Hasan, S.S., Deng, X., 2020. Examining the impacts of future land use/land cover changes on climate in Punjab province, Pakistan: implications for environmental sustainability and economic growth. *Environmental Science and Pollution Research* 27, 25415-25433.
- Shamsolmoali, P., Zareapoor, M., Zhou, H., Wang, R., Yang, J., 2020. Road segmentation for remote sensing images using adversarial spatial pyramid networks. *IEEE Transactions on Geoscience and Remote Sensing*.
- Sherrah, J., 2016. Fully convolutional networks for dense semantic labelling of high-resolution aerial imagery. *arXiv preprint arXiv:1606.02585*.
- Srinivas, A., Lin, T.-Y., Parmar, N., Shlens, J., Abbeel, P., Vaswani, A., 2021. Bottleneck transformers for visual recognition, *Proceedings of the IEEE/CVF Conference on Computer Vision and Pattern Recognition*, pp. 16519-16529.
- Tan, M., Pang, R., Le, Q.V., 2020. Efficientdet: Scalable and efficient object detection, *Proceedings of the IEEE/CVF conference on computer vision and pattern recognition*, pp. 10781-10790.
- Vaswani, A., Shazeer, N., Parmar, N., Uszkoreit, J., Jones, L., Gomez, A.N., Kaiser, Ł., Polosukhin, I., 2017.

- Attention is all you need, *Advances in neural information processing systems*, pp. 5998-6008.
- Wang, L., Li, R., Duan, C., Zhang, C., Meng, X., Fang, S., 2021a. A Novel Transformer based Semantic Segmentation Scheme for Fine-Resolution Remote Sensing Images. *arXiv preprint arXiv:2104.12137*.
- Wang, L., Li, R., Wang, D., Duan, C., Wang, T., Meng, X., 2021b. Transformer Meets Convolution: A Bilateral Awareness Network for Semantic Segmentation of Very Fine Resolution Urban Scene Images. *Remote Sensing* 13, 3065.
- Wang, X., Girshick, R., Gupta, A., He, K., 2018. Non-local neural networks, *Proceedings of the IEEE conference on computer vision and pattern recognition*, pp. 7794-7803.
- Xu, W., Xu, Y., Chang, T., Tu, Z., 2021. Co-scale conv-attentional image transformers. *arXiv preprint arXiv:2104.06399*.
- Yang, M.Y., Kumaar, S., Lyu, Y., Nex, F., 2021. Real-time Semantic Segmentation with Context Aggregation Network. *ISPRS Journal of Photogrammetry and Remote Sensing* 178, 124-134.
- Yin, H., Pflugmacher, D., Li, A., Li, Z., Hostert, P., 2018. Land use and land cover change in Inner Mongolia-understanding the effects of China's re-vegetation programs. *Remote Sensing of Environment* 204, 918-930.
- Yu, C., Wang, J., Peng, C., Gao, C., Yu, G., Sang, N., 2018. Bisenet: Bilateral segmentation network for real-time semantic segmentation, *Proceedings of the European conference on computer vision (ECCV)*, pp. 325-341.
- Yuan, Y., Chen, X., Wang, J., 2020. Object-contextual representations for semantic segmentation, *Computer Vision—ECCV 2020: 16th European Conference, Glasgow, UK, August 23–28, 2020, Proceedings, Part VI* 16. Springer, pp. 173-190.
- Zhang, C., Atkinson, P.M., George, C., Wen, Z., Diazgranados, M., Gerard, F., 2020a. Identifying and mapping individual plants in a highly diverse high-elevation ecosystem using UAV imagery and deep learning. *ISPRS Journal of Photogrammetry and Remote Sensing* 169, 280-291.
- Zhang, C., Harrison, P.A., Pan, X., Li, H., Sargent, I., Atkinson, P.M., 2020b. Scale Sequence Joint Deep Learning (SS-JDL) for land use and land cover classification. *Remote Sensing of Environment* 237, 111593.
- Zhang, Q., Yang, Y., 2021. ResT: An Efficient Transformer for Visual Recognition. *arXiv preprint arXiv:2105.13677*.
- Zhao, H., Shi, J., Qi, X., Wang, X., Jia, J., 2017. Pyramid scene parsing network, *Proceedings of the IEEE conference on computer vision and pattern recognition*, pp. 2881-2890.
- Zheng, S., Lu, J., Zhao, H., Zhu, X., Luo, Z., Wang, Y., Fu, Y., Feng, J., Xiang, T., Torr, P.H., 2021. Rethinking semantic segmentation from a sequence-to-sequence perspective with transformers, *Proceedings of the IEEE/CVF Conference on Computer Vision and Pattern Recognition*, pp. 6881-6890.
- Zhou, Z., Siddiquee, M.M.R., Tajbakhsh, N., Liang, J., 2018. Unet++: A nested u-net architecture for medical image segmentation, *Deep Learning in Medical Image Analysis and Multimodal Learning for Clinical Decision Support*. Springer, pp. 3-11.
- Zhu, X., Su, W., Lu, L., Li, B., Wang, X., Dai, J., 2020. Deformable DETR: Deformable Transformers for End-to-End Object Detection. *arXiv preprint arXiv:2010.04159*.
- Zhu, X.X., Tuia, D., Mou, L., Xia, G.-S., Zhang, L., Xu, F., Fraundorfer, F., 2017. Deep learning in remote sensing: A comprehensive review and list of resources. *IEEE Geoscience and Remote Sensing Magazine* 5, 8-36.
- Zhuang, J., Yang, J., Gu, L., Dvornek, N., 2019. Shelfnet for fast semantic segmentation, *Proceedings of the IEEE/CVF International Conference on Computer Vision Workshops*, pp. 0-0.

